Journal of Zhejiang University-SCIENCE A (Applied Physics & Engineering) 2024 25(5):382-394
www.jzus.zju.edu.cn; www.springer.com/journal/11582
E-mail: jzus_a@zju.edu.cn

Research Article

https://doi.org/10.1631/jzus.A2300651

Two simple memristive maps with adaptive energy regulation and digital signal process verification

Feifei YANG[1], Lujie REN[3], Jun MA[1,2]✉, Zhigang ZHU[2]

[1]*College of Electrical and Information Engineering, Lanzhou University of Technology, Lanzhou 730050, China*
[2]*Department of Physics, Lanzhou University of Technology, Lanzhou 730050, China*
[3]*School of Information Science and Engineering, Dalian Polytechnic University, Dalian 116034, China*

Abstract: Mathematical models can produce desired dynamics and statistical properties with the insertion of suitable nonlinear terms, while energy characteristics are crucial for practical application because any hardware realizations of nonlinear systems are relative to energy flow. The involvement of memristive terms relative to memristors enables multistability and initial-dependent property in memristive systems. In this study, two kinds of memristors are used to couple a capacitor or an inductor, along with a nonlinear resistor, to build different neural circuits. The corresponding circuit equations are derived to develop two different types of memristive oscillators, which are further converted into two kinds of memristive maps after linear transformation. The Hamilton energy function for memristive oscillators is obtained by applying the Helmholz theorem or by mapping from the field energy of the memristive circuits. The Hamilton energy functions for both memristive maps are obtained by replacing the gains and discrete variables for the memristive oscillator with the corresponding parameters and variables. The two memristive maps have rich dynamic behaviors including coherence resonance under noisy excitation, and an adaptive growth law for parameters is presented to express the self-adaptive property of the memristive maps. A digital signal process (DSP) platform is used to verify these results. Our scheme will provide a theoretical basis and experimental guidance for oscillator-to-map transformation and discrete map-energy calculation.

Key words: Hamilton energy; Discrete memristor; Self-adaptive regulation; Digital signal process (DSP) implementation

1 Introduction

In 1971, Leon Chua predicted the existence of the fourth fundamental electronic component, which is known as a memristor (Chua, 1971). Memristors can be magnetic flux-dependent (Batas and Fiedler, 2011; Li et al., 2021; Vignesh et al., 2024) or charge-controlled types (Chandía et al., 2018; Isah et al., 2020; Sun et al., 2023). They are nonlinear resistors (NRs) with memory characteristics. A nonlinear circuit with a memristor exhibits complex nonlinear dynamic behaviors. For example, Xu et al. (2016) designed a improved memristive Chua circuit by applying a non-ideal active voltage-controlled memristor to replace the Chua's diode of the Chua circuit. The result indicated that the improved memristive Chua circuit had multiple attractors with multistability. Guo et al. (2022) incorporated a magnetic flux-regulated memristor into different branches of a Chua circuit to explore the influence of magnetic field on the output state of the circuit. Ye et al. (2020) designed a multiple memristors chaotic circuit, and used the circuit for an image-encryption algorithm. A four-variable memristive oscillator and nonlinear control were investigated by Gokyildirim et al. (2022). Njimah et al. (2023) suggested a chaotic system with four-scroll chaotic attractors. Because memristors can simulate synaptic weight-regulation behavior and pulse-timing-dependent synaptic plasticity, memristors are widely used in artificial synapses and neural networks. Examples include the electric-field-sensitive memristor neuron model (Yang et al., 2023c), the electromagnetic-sensitive and electric-field-sensitive memristor neuron model (Yang

✉ Jun MA, hyperchaos@lut.edu.cn
Feifei YANG, https://orcid.org/0000-0002-1649-1225
Lujie REN, https://orcid.org/0000-0002-6906-3259
Jun MA, https://orcid.org/0000-0002-6127-000X

Received Dec. 25, 2023; Revision accepted Feb. 10, 2024;
Crosschecked Mar. 1, 2024; Online first Apr. 3, 2024

et al., 2023a), memristive neural networks (Pham et al., 2016; Pedretti et al., 2017; Wang et al., 2018; Smagulova and James, 2019; Bao H et al., 2020; Yang et al., 2023b), and memristive synapses (Covi et al., 2016; Boybat et al., 2018; Juzekaeva et al., 2019; Wu et al., 2022; Lin et al., 2023).

Recently, application of discrete memristors has become a research hotspot. Discrete memristors can be obtained by applying the forward Euler difference algorithm (Bao BC et al., 2020). Previously, many discrete memristive maps have been proposed, for example, 2D discrete memristor maps (Deng and Li, 2021, 2022; Bao BC et al., 2023), a 3D discrete memristor map (Lai and Yang, 2023), discrete memristive hyperchaotic maps (Fan et al., 2023; Ma et al., 2023; Ren et al., 2023), discrete memristive neuron maps (Ramakrishnan et al., 2022; Mehrabbeik et al., 2023; Xu et al., 2023), a discrete memristive map based on multiple nonlinear terms (Hoang et al., 2023), a discrete memristive map without a fixed point (Ramadoss et al., 2022), and a discrete memristive map with asymmetry (Pham et al., 2024). Zhao et al. (2023) designed fully fixed-point digital integrated circuits of discrete memristive maps, which provided a foundation for the further application of discrete memristor maps. Most of the suggested discrete memristors and maps have been proposed from mathematical forms rather than by clarifying their physical properties in a theoretical way. Physical modeling of discrete memristor maps is not perfect, and is generally obtained by introducing discrete memristors into existing discrete maps. The energy of discrete memristor maps is also an open problem.

Inspired by the suggestion in (Ma, 2024) that biophysical and memristive maps can be converted from memristive circuits, we decided to define the energy function in a theoretical way. In this work, we constructed two simple memristive circuits by using two kinds of memristor elements, an NR, and either a capacitor or an inductor. The two simplest memristive oscillators were derived and their Hamilton energy functions were obtained with a physical approach. Based on the transformation relationship between the oscillator and map, as described in (Guo et al., 2023b), we obtained two different types of memristive maps and the corresponding Hamilton energy functions. The results provide possible guidance for designing discrete maps and calculating energy.

2 Model and scheme

From a physical viewpoint, continuous energy exchange is crucial to support oscillation in a circuit, and connection to nonlinear elements is effective in triggering nonlinear behaviors. Therefore, both capacitive and inductive components and nonlinear elements are required to build an oscillatory circuit for generating different firing modes. We constructed a simple memristive circuit using a memristor element, an NR, and a capacitor, as shown in Fig. 1 (Case 1).

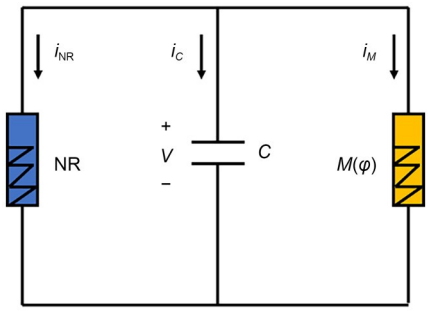

Fig. 1 Simple magnetic flux-controlled memristor (MFCM) circuit. $M(\varphi)$ denotes an MFCM, and C is a capacitor

In Fig. 1, the current of the NR branch in the circuit is estimated by

$$i_{\mathrm{NR}}=-\frac{r}{\rho}\left(V-\frac{V^2}{V_0}\right), \tag{1}$$

where ρ denotes the resistance within the linear region, V_0 is a cut-off voltage, and r is a dimensionless gain. The physical properties of the memristor with controllable parameters can be estimated by

$$\begin{cases} i_M=M(\varphi)V_M=\varphi V, \\ \dfrac{\mathrm{d}\varphi}{\mathrm{d}t}=\alpha\varphi+\beta V. \end{cases} \tag{2}$$

According to Kirchhoff's laws, the circuit equations for the memristive circuit in Fig. 1 can be described as follows:

$$\begin{cases} C\dfrac{\mathrm{d}V}{\mathrm{d}t}=\dfrac{r}{\rho}\left(V-\dfrac{V^2}{V_0}\right)-\varphi V, \\ \dfrac{\mathrm{d}\varphi}{\mathrm{d}t}=\alpha\varphi+\beta V. \end{cases} \tag{3}$$

Dimensionless parameters and variables are defined for Eq. (3) as follows:

$$\begin{cases} x=\dfrac{V}{V_0},\ w=\dfrac{\varphi}{\rho C V_0},\ \tau=\dfrac{t}{\rho C}, \\ c=\rho^2 C V_0,\ a=\alpha\rho C. \end{cases} \tag{4}$$

Physical equations in Eq. (3) can be updated by

$$\begin{cases} \dfrac{\mathrm{d}x}{\mathrm{d}t}=r(x-x^2)-cwx, \\ \dfrac{\mathrm{d}w}{\mathrm{d}t}=aw+\beta x. \end{cases} \tag{5}$$

The field energy for the electric components in Fig. 1 and the dimensionless energy H_1 are derived by

$$\begin{cases} W_1=\dfrac{1}{2}CV^2+\dfrac{1}{2}L_M i_M^2=\dfrac{1}{2}CV^2+\dfrac{1}{2}\varphi i_M, \\ H_1=\dfrac{W_1}{CV_0^2}=\dfrac{1}{2}x^2+\dfrac{1}{2}cw^2x. \end{cases} \tag{6}$$

The same Hamilton energy function is confirmed for Eq. (3) by applying Helmholtz's theorem. The equation for the memristive oscillator can then be rewritten in a vector form, as follows:

$$\begin{aligned} \begin{pmatrix} \dot{x} \\ w \end{pmatrix} &= \begin{pmatrix} r(x-x^2)-cwx \\ aw+\beta x \end{pmatrix} = \boldsymbol{F}_{\mathrm{c}}+\boldsymbol{F}_{\mathrm{d}} = \begin{pmatrix} -\beta cwx \\ \beta x+0.5\beta cw^2 \end{pmatrix} + \\ &\begin{pmatrix} r(x-x^2)-cwx(1-\beta) \\ aw-0.5\beta cw^2 \end{pmatrix} = \begin{pmatrix} 0 & -\beta \\ \beta & 0 \end{pmatrix} \begin{pmatrix} x+0.5cw^2 \\ cwx \end{pmatrix} + \\ &\begin{pmatrix} \dfrac{r(x-x^2)-cwx(1-\beta)}{x+0.5cw^2} & 0 \\ 0 & \dfrac{aw-0.5\beta cw^2}{cwx} \end{pmatrix} \begin{pmatrix} x+0.5cw^2 \\ cwx \end{pmatrix}. \end{aligned} \tag{7}$$

According to Helmholtz's theorem, the Hamilton energy function H_1 meets the following criterion:

$$\begin{cases} \nabla \boldsymbol{H}_1^{\mathrm{T}} \boldsymbol{F}_{\mathrm{c}} = -\beta cwx \dfrac{\partial H_1}{\partial x} + \\ \qquad (\beta x+0.5\beta cw^2)\dfrac{\partial H_1}{\partial w}=0, \\ \dfrac{\mathrm{d}H_1}{\mathrm{d}\tau}=r(x-x^2)(x+0.5cw^2)- \\ \qquad cwx(x-\beta x-aw+0.5cw^2)=\nabla \boldsymbol{H}_1^{\mathrm{T}} \boldsymbol{F}_{\mathrm{d}}. \end{cases} \tag{8}$$

Indeed, the energy function H_1 in Eq. (6) matches the criterion in Eq. (8) completely. Furthermore, the linear transformation is imposed on the sampled time series for variables from Eq. (5).

$$\begin{cases} y_n=\dfrac{r\Delta\tau}{1+r\Delta\tau}x_n,\ z_n=\dfrac{r\Delta\tau}{1+r\Delta\tau}w_n,\ \mu=b\Delta\tau, \\ \lambda=1+r\Delta\tau,\ \delta=a\Delta\tau+1,\ \gamma=c\Delta\tau, \end{cases} \tag{9}$$

where $\Delta\tau$ is the time step for numerical approach of Eq. (5), and a memristive map is proposed by

$$\begin{cases} y_{n+1}=\lambda(y_n-y_n^2)-\gamma y_n z_n, \\ z_{n+1}=\delta y_n+\mu z_n. \end{cases} \tag{10}$$

Applying the same weights for two terms in the discrete energy function for Eq. (6), the Hamilton energy for the memristor map in Eq. (10) can be estimated by

$$H_n=\frac{1}{2}y_n+\frac{1}{2}\gamma z_n^2 y_n. \tag{11}$$

To investigate the self-adaptation of a memristive map, one parameter for the map must be controlled by the energy flux in an adaptive growth law:

$$\begin{cases} \mu_{n+1}=\mu_n+k\cdot\theta(p-H_n), \\ \theta(\cdot)=1,\ p\geqslant 0, \\ \theta(\cdot)=0,\ p<0. \end{cases} \tag{12}$$

where the threshold $0<p<1$ determines the total energy of the memristive map in the nth iteration. μ_n is the value for the memristive parameter in the nth iteration, the parameter k is the growth step, and the Heaviside function θ is used to control parameter growth. Other parameters in Eq. (10) should be adjustable by similar laws in Eq. (12).

The second case is that a simple memristive circuit is obtained by applying a charge-controlled memristor (CCM), an NR, and an inductor. The corresponding scheme diagram of the circuit is displayed in Fig. 2 (Case 2).

In Fig. 2, the voltage of the NR branch in the circuit can be estimated by

$$V_{\mathrm{NR}}=r\rho\left(i_L-\frac{\rho i_L^2}{V_0}\right), \tag{13}$$

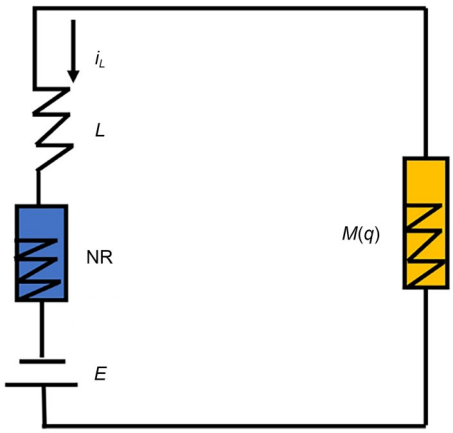

Fig. 2 Simple CCM circuit. *M*(*q*) denotes a CCM, *L* is an inductor, and *E* is a constant voltage source

where the parameters (ρ, V_0, and r) have the same definitions as in Eq. (1). The physical relation for the memristor is

$$\begin{cases} V_M = M(q)\, i_L = (\alpha + 3\beta q^2)\, i_L, \\ \dfrac{\mathrm{d}q}{\mathrm{d}t} = aq + bi_L. \end{cases} \tag{14}$$

The relations between physical variables for the memristive circuit in Case 2 are expressed by

$$\begin{cases} L\dfrac{\mathrm{d}i_L}{\mathrm{d}t} = r\rho\left(i_L - \dfrac{\rho i_L^2}{V_0}\right) - (\alpha + 3\beta q^2)\, i_L - E, \\ \dfrac{\mathrm{d}q}{\mathrm{d}t} = aq + bi_L. \end{cases} \tag{15}$$

Similar definitions for dimensionless variables and parameters are given in

$$\begin{cases} y = \dfrac{\rho i_L}{V_0},\ u = \dfrac{\rho^2 q}{LV_0},\ \tau = \dfrac{\rho t}{L},\ \alpha' = \dfrac{\alpha}{\rho}, \\ \beta' = \dfrac{3\beta L^2 V_0^2}{\rho^5},\ a' = \dfrac{aL}{\rho},\ d = \dfrac{E}{V_0}. \end{cases} \tag{16}$$

By inserting Eq. (16) into Eq. (15), a new memristive oscillator for Case 2 can be obtained by

$$\begin{cases} \dfrac{\mathrm{d}y}{\mathrm{d}t} = r(y - y^2) - (\alpha' + \beta' u^2)\, y - d, \\ \dfrac{\mathrm{d}u}{\mathrm{d}t} = a'u + by. \end{cases} \tag{17}$$

The physical field energy for the electric component in Case 2 and the dimensionless energy H_2 are derived by

$$\begin{cases} W_2 = \dfrac{1}{2}Li_L^2 + \dfrac{1}{2}C_M V_M^2 = \dfrac{1}{2}Li_L^2 + \dfrac{1}{2}qV_M, \\ H_2 = \dfrac{W_2}{V_0^2 \dfrac{L}{\rho^2}} = \dfrac{1}{2}y^2 + \dfrac{1}{2}(\alpha' + \beta' u^2)\, uy. \end{cases} \tag{18}$$

The Hamilton energy function for Eq. (17) is calculated by applying Helmholtz's theorem, and the mathematical proof is as follows:

$$\begin{aligned} &\begin{pmatrix} \dot{y} \\ \dot{u} \end{pmatrix} = \begin{pmatrix} r(y - y^2) - (\alpha' + \beta' u^2)\, y - d \\ a'u + by \end{pmatrix} = \\ &\boldsymbol{F}_{\mathrm{c}} + \boldsymbol{F}_{\mathrm{d}} = \begin{pmatrix} -0.5by(\alpha' + 3\beta' u^2) \\ by + 0.5b(\alpha' u + \beta' u^3) \end{pmatrix} + \\ &\begin{pmatrix} r(y - y^2) - (\alpha' + \beta' u^2)\, y(1 - 0.5b) - d \\ a'u - 0.5b(\alpha' u + \beta' u^3) \end{pmatrix} = \\ &\begin{pmatrix} 0 & -b \\ b & 0 \end{pmatrix} \begin{pmatrix} y + 0.5(\alpha' u + \beta' u^3) \\ 0.5y(\alpha' + 3\beta' u^2) \end{pmatrix} + \\ &\begin{pmatrix} a_{11} & 0 \\ 0 & a_{22} \end{pmatrix} \begin{pmatrix} y + 0.5(\alpha' u + \beta' u^3) \\ 0.5y(\alpha' + 3\beta' u^2) \end{pmatrix}, \\ &a_{11} = \frac{r(y - y^2) - (\alpha' + \beta' u^2)\, y(1 - 0.5b) - d}{y + 0.5(\alpha' u + \beta' u^3)}, \\ &a_{22} = \frac{a'u - 0.5b(\alpha' u + \beta' u^3)}{0.5y(\alpha' + 3\beta' u^2)}. \end{aligned} \tag{19}$$

The Hamilton energy function H_2 meets the following criterion:

$$\begin{cases} \nabla \boldsymbol{H}_2^{\mathrm{T}} \boldsymbol{F}_{\mathrm{c}} = -0.5by(\alpha' + 3\beta' u^2) \dfrac{\partial H_2}{\partial y} + \\ \qquad \left[by + 0.5b(\alpha' u + \beta' u^3)\right] \dfrac{\partial H_2}{\partial u} = 0, \\ \dfrac{\mathrm{d}H_2}{\mathrm{d}\tau} = r(y - y^2)\left[y + 0.5(\alpha' u + \beta' u^3)\right] - \\ \qquad y(\alpha' u + \beta' u^2)\left[y + 0.5(\alpha' u + \beta' u^3)\right] - \\ \qquad d\left[y + 0.5(\alpha' u + \beta' u^3)\right] + \\ \qquad (by + \alpha' u)\left[0.5y(\alpha' + 3\beta' u^2)\right] = \nabla \boldsymbol{H}_2^{\mathrm{T}} \boldsymbol{F}_{\mathrm{d}}. \end{cases} \tag{20}$$

Similar linear transformation is used for the sampled variables in Eq. (17), involving a time step as follows:

$$\begin{cases} w_n=\dfrac{r\Delta\tau}{1+r\Delta\tau}y_n,\ v_n=\dfrac{r\Delta\tau}{1+r\Delta\tau}u_n, \\ \chi=1+r\Delta\tau,\ \xi=\alpha'\Delta\tau, \\ \varepsilon=\dfrac{\beta'(1+r\Delta\tau)^2}{r^2\Delta\tau},\ \kappa=a\Delta\tau+1, \\ \eta=b\Delta\tau,\ d'=d\Delta\tau, \end{cases} \tag{21}$$

where $\Delta\tau$ is the time step for the numerical approach used in Eq. (17). A new memristive map is given in

$$\begin{cases} w_{n+1}=\chi(w_n-w_n^2)-(\xi+\varepsilon v_n^2)w_n-d', \\ v_{n+1}=\kappa w_n+\eta v_n. \end{cases} \tag{22}$$

The Hamilton energy for the memristive map in Eq. (22) is estimated by

$$H_n'=\frac{1}{2}w_n+\frac{1}{2}(\xi+\varepsilon v_n^2)w_n v_n. \tag{23}$$

A similar growth criterion for one parameter in the map is controlled by the energy level as follows:

$$\begin{cases} \eta_{n+1}=\eta_n+k\cdot\theta(p-H_n'), \\ \theta(\cdot)=1,\ p\geqslant 0, \\ \theta(\cdot)=0,\ p<0, \end{cases} \tag{24}$$

where η_n is the value for the memristive parameter in the nth iteration. The threshold p controls the mode transition in the firing modes.

3 Results and discussion

In this section, we describe how we investigated the dynamic behaviors of the memristive maps (magnetic flux-controlled memristor (MFCM) and CCM) by changing the map parameters. First, the parameters for the memristive map presented in Eq. (10) were selected as λ=3.9, γ=0.12, and μ=0.4, and the initial values were fixed at (0.1, 0.1). The parameter δ was changed from 1.0 to 3.0, and the bifurcation diagram and Lyapunov exponents for the map are shown in Fig. 3a. By applying the same parameters and initial values, the parameter δ=1.5 and the parameter μ increased from 0.3 to 0.7. The results are displayed in Fig. 3b.

We observed that the MFCM map presented in Eq. (10) produced complex dynamic characteristics when we changed one parameter continuously, for example, the period doubling bifurcation to chaos appears. As the parameter values increased, the MFCM map in Eq. (10) started from chaos and entered into period states through reverse period doubling, and some narrow periodic windows appeared. To allow readers to more clearly observe the phase trajectories corresponding to different parameter values for the

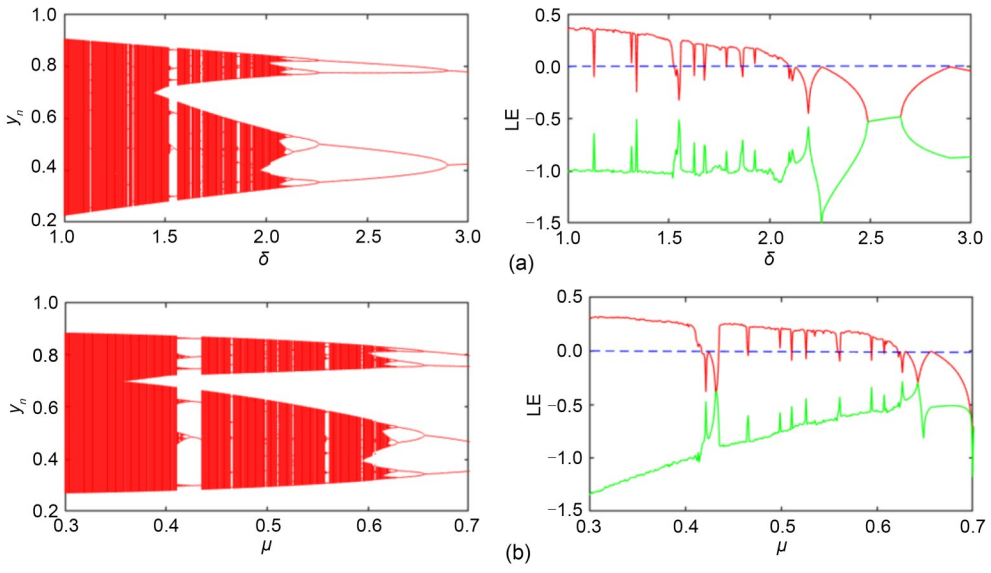

Fig. 3 Bifurcation diagram and two-Lyapunov exponent (LE) spectrum after changing one parameter: (a) λ=3.9, γ=0.12, μ=0.4; (b) λ=3.9, γ=0.12, δ=1.5. The initial values are (0.1, 0.1)

memristive map, the phase trajectories corresponding to different values for parameter δ are shown in Fig. 4.

The results in Fig. 4 show that the MFCM map in Eq. (10) can be induced to exhibit complex dynamic behaviors (periodic, chaotic) by changing parameter δ, and they are consistent with the dynamics presented in Fig. 3a. Furthermore, we analyzed the Hamilton energy values for different output states. By using the same parameters and initial values, the iterative sequences of variables and Hamilton energy could be plotted in Figs. 5 and 6, respectively.

Our findings confirm that the memristive map presenting in chaos has a smaller average Hamilton energy value, while it retains a higher mean Hamilton

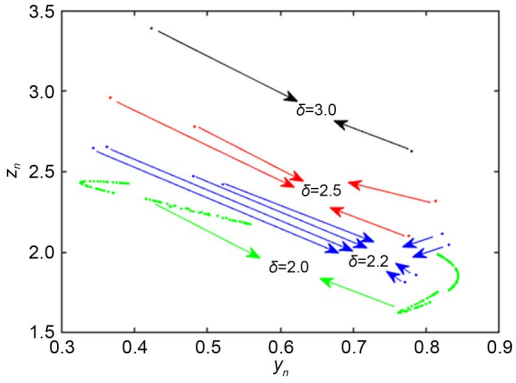

Fig. 4 Phase diagram with different values for the parameter δ when the parameters are fixed at λ=3.9, γ=0.12, and μ=0.4, and the initial values are (0.1, 0.1)

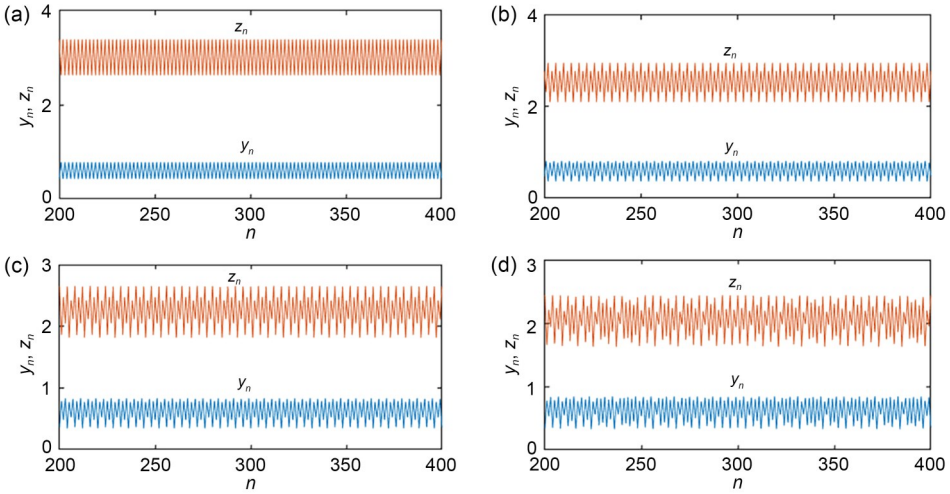

Fig. 5 Evolution of variables with different values for parameter δ: (a) δ=3.0; (b) δ=2.5; (c) δ=2.2; (d) δ=2.0. Parameters are set as λ=3.9, γ=0.12, and μ=0.4, and the initial values are (0.1, 0.1)

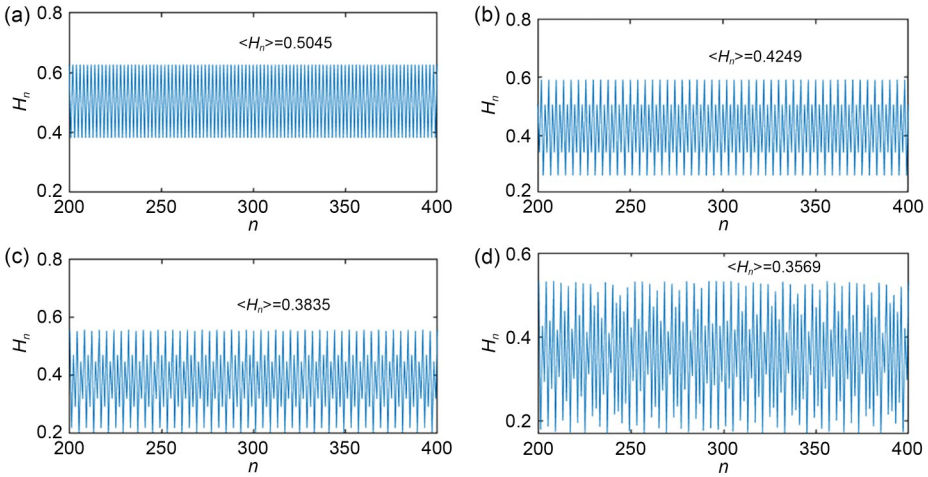

Fig. 6 Changes in Hamilton energy with different values for parameter δ: (a) δ=3.0; (b) δ=2.5; (c) δ=2.2; (d) δ=2.0. Parameters are set as λ=3.9, γ=0.12, and μ=0.4, and the initial values are (0.1, 0.1). <H_n> denotes the mean value of Hamilton energy

energy value in the periodic state. In addition, the mean Hamilton energy of the memristor map decreases as the period number increases.

Based on the criterion of growth for the parameter μ described by Eq. (12), the threshold was fixed at p=0.5 and the gain at k=0.005. The parameters were kept at λ=3.9, γ=0.12, and δ=2.0, and the initial values were (0.1, 0.1). The parameter started its growth from μ_1=0.3 and the memristive map presented in Eq. (10) was iterated 200 times. The iterative sequence for the growth of parameter μ, sampled time series for Hamilton energy, iterative sequence of variables, and phase diagram are shown in Fig. 7.

The results, as shown in Fig. 7, revealed that the parameter μ of the memristive map reached a stable value of 0.71 through 140 iterations. The Hamilton energy and the variables were transferred from chaotic patterns to periodic states, and a similar shift occurred in the phase diagram. This result is consistent with the results of dynamic behavior analysis as shown in Fig. 3. In addition, the dynamic behaviors in Eq. (22) were explored with the same initial values (0.1, 0.1). The parameters selected were χ=3.9, ξ=0.01, and ε=0.1. Bifurcation analysis and dependence of Lyapunov exponents on parameters (d', κ, η) in the memristive map are plotted in Fig. 8.

Similar to the results in Fig. 3, the memristive map in Eq. (22) started from chaos and entered into periodic states through reverse period doubling when the parameter values increased, and some narrow periodic windows occurred. The phase diagrams for different parameters are shown in Fig. 9.

The results shown in Fig. 9 indicate that the dynamics for the memristive map (Case 2) can be adjusted by changing the parameters. The evolution of the iterative sequences of variables and Hamilton energy are displayed in Figs. 10 and 11, respectively.

Similar to the case for an MFCM memristive map, the CCM-based map has a smaller mean Hamilton energy value in a chaotic state, but a higher mean Hamilton energy value in a periodic state. In addition, the mean Hamiltonian energy of the memristive map decreases as the period number increases.

According to the criterion of growth for the parameter η described by Eq. (24), we set the threshold p=0.5 and the gain k=0.005; we kept the parameters as χ=3.9, ξ=0.01, ε=0.1, d'=0, and κ=1, and applied the same initial values (0.1, 0.1). The parameter began its growth at η_1=0.1, the memristive map presented in Eq. (22) was iterated 200 times, and the growth of parameter η, changes in Hamilton energy, variables, and phase diagram are shown in Fig. 12.

The results confirmed that the parameter η of the memristive map relative to CCM reached a stable value of 0.73 after 140 iterations. The Hamilton energy and the variables began from chaotic patterns and transformed to periodic states, and a similar shift occurred in the phase diagram. This indicates that the dynamics for memristive maps can be adapt-controlled by energy flow.

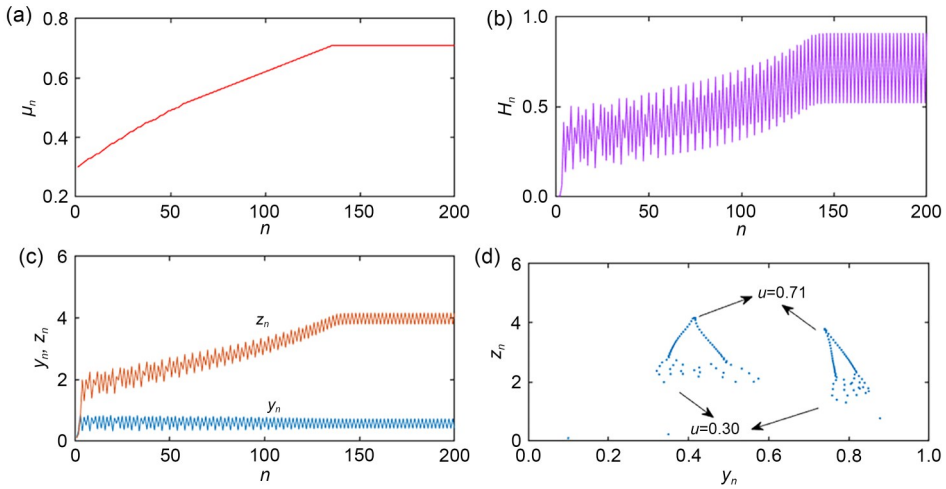

Fig. 7 Evolution of variables, parameters, and energy: (a) growth of parameter μ; (b) Hamilton energy; (c) output variables; (d) phase diagram. Parameters are set as λ=3.9, γ=0.12, δ=2.0, μ_1=0.3, p=0.5, and k=0.005, and the initial values are (0.1, 0.1)

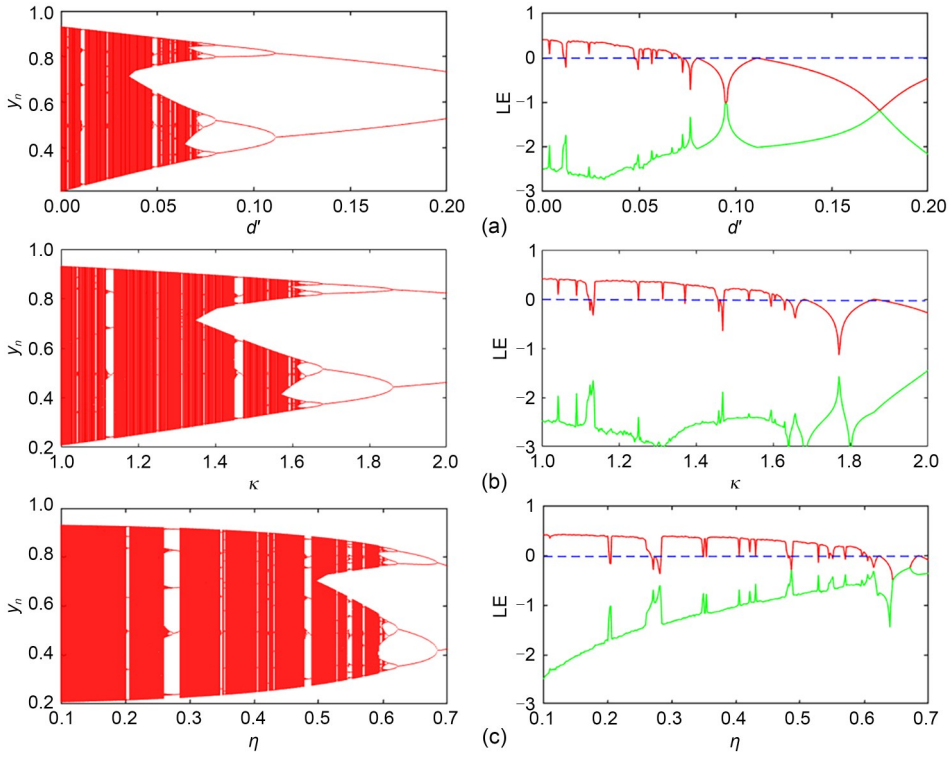

Fig. 8 Bifurcation diagram and Lyapunov exponent spectrum with adjustment of one parameter: (a) χ=3.9, ξ=0.01, ε=0.1, η=0.1, κ=1; (b) χ=3.9, ξ=0.01, ε=0.1, d'=0, η=0.1; (c) χ=3.9, ξ=0.01, ε=0.1, d'=0, κ=1

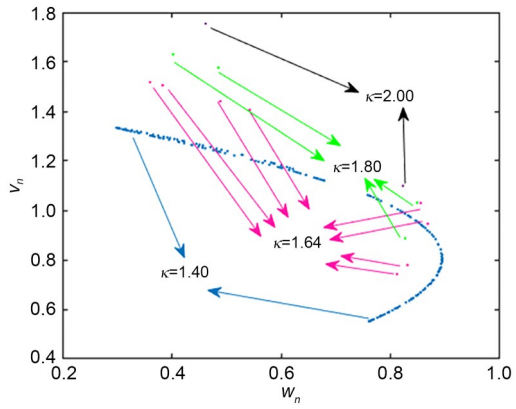

Fig. 9 Phase diagram with different parameters κ. Parameters are set as χ=3.9, ξ=0.01, ε=0.1, d'=0, and η=0.1, and the initial values are (0.1, 0.1)

To further verify the application of new memristive maps in the digital signal process, we implemented the two simple memristive maps on a digital signal-process (DSP) platform. In the tests, the core processing chip was TMS320F28335, with a 16-bit D/A convert (DAC8552) and other circuit elements. The hardware frame diagram is plotted in Fig. 13.

The parameters of the MFCM memristive map are λ=3.9, γ=0.12, μ=0.4, and δ=2, and the initial values are (0.1, 0.1). The parameters of the MFCM map are χ=3.9, ξ=0.01, ε=0.1, κ=1.4, d'=0, and η=0.1, and the initial values are (0.1, 0.1). The experimental device and results are shown in Fig. 14.

Fig. 14 proved the feasibility of hardware implementation of the simple memristive maps.

To summarize, we developed two memristive maps from two simple nonlinear memristive circuits, and clarified their physical properties (including energy level and adaptive controllability by parameter and mode selection). The memristive maps with simple forms exhibit rich dynamic behaviors, and their mean Hamiltonian energy value decreases as the period number increases. Similar to nonlinear oscillators, the Hamilton energy functions for discrete maps depend on the maps' parameters and output variables. When the firing mode is switched, energy shift is induced by detecting the average energy levels. The adaptive growth law of bifurcation parameters accounts for the role of energy regulation. The simple memristive maps investigated here can be implemented on a DSP platform. In most previous studies, dynamics of memristive oscillators were investigated (Chen et al., 2020; Liu et al., 2021; Bao et al., 2022; Wu et al., 2023; Wu

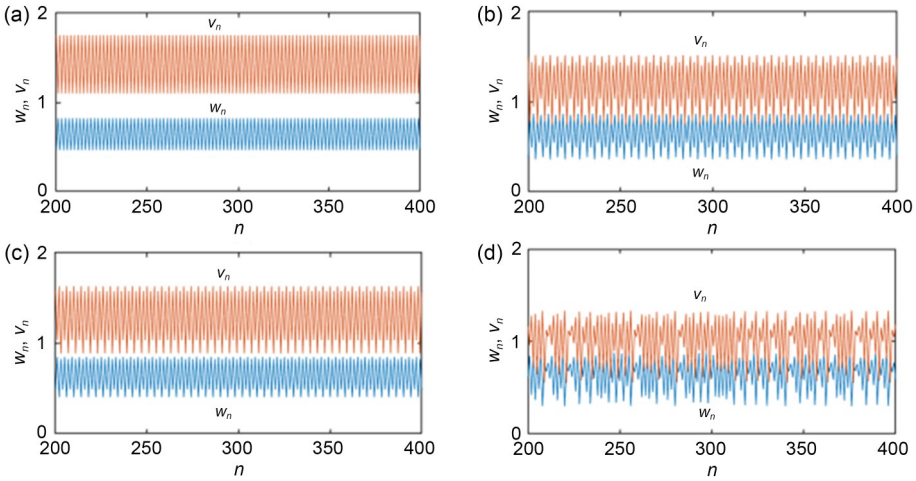

Fig. 10 Changes in variables with different values of parameter κ: (a) κ=2.00; (b) κ=1.80; (c) κ=1.64; (d) κ=1.40. Parameters are set as χ=3.9, ξ=0.01, ε=0.1, d'=0, and η=0.1, and the initial values are (0.1, 0.1)

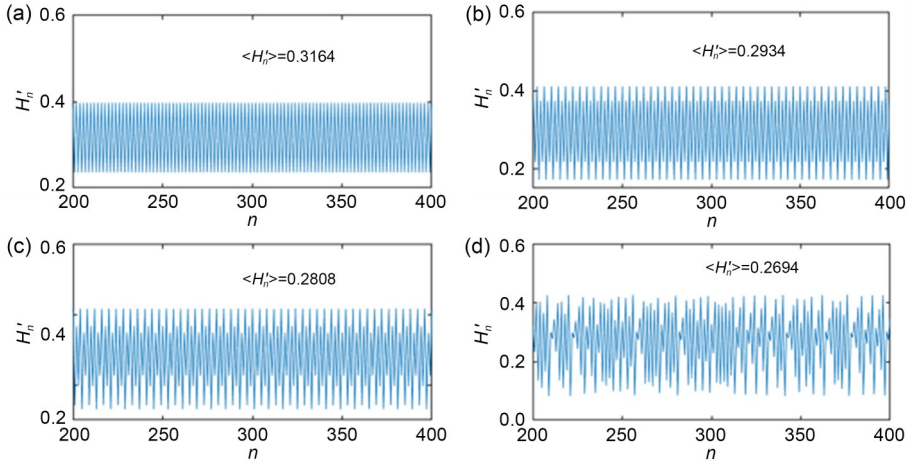

Fig. 11 Evolution of Hamilton energy with different values of parameter κ: (a) κ=2.00; (b) κ=1.80; (c) κ=1.64; (d) κ=1.40. Parameters are set as χ=3.9, ξ=0.01, ε=0.1, d'=0, and η=0.1, and the initial values are (0.1, 0.1). <H_n'> denotes the mean value of Hamilton energy

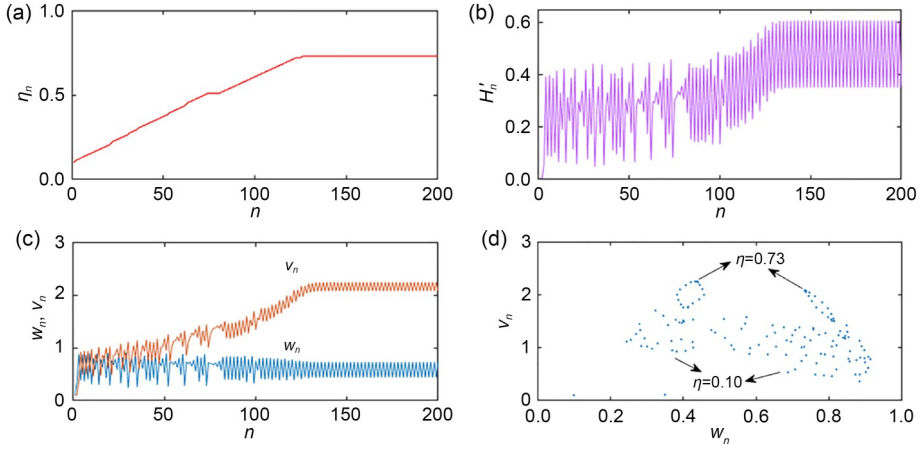

Fig. 12 Evolution of variables, parameters, and energy: (a) parameter η; (b) Hamilton energy; (c) output variables; (d) phase diagram. Parameters are set as χ=3.9, ξ=0.01, ε=0.1, κ=1, d'=0, η_1=0.1, p=0.5, and k=0.005, and the initial values are (0.1, 0.1)

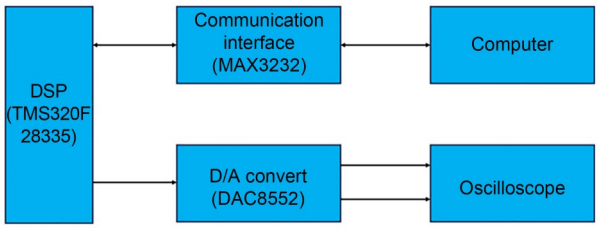

Fig. 13 Hardware frame diagram of DSP implementation. TMS320F28335 is a 32-bit floating point DSP processor, and the maximum clock frequency is 150 MHz

and Yao, 2023). Meanwhile, dynamics of memristive maps have been explored in terms of mathematical definitions and with a numerical approach, accompanied by suitable implementation of analog circuits (Deng and Li, 2021; Ma et al., 2022; Zhong et al., 2022; Bao H et al., 2023; Hou et al., 2023). Based on our suggested memristive maps, more memristive neurons in map form can be examined to explore the DSP and logic operation. In particular, these maps, which have clear physical descriptions, can be used for computational neuroscience and functional brain networks to predict neural disease (Liu et al., 2022a, 2022b; Yu et al., 2023).

From a dynamic viewpoint, both nonlinear oscillators and maps can be tamed to prevent spiking and bursting behaviors, and some of them can be produced with analog circuits or digital circuits. For oscillator-like neurons, equivalent neural circuits can be designed by connecting capacitive, inductive, and memristive elements in some loops. Map-based neurons (Luo and Flanagan, 2007; Ibarz et al., 2011; Zandi-Mehran et al., 2020; Ramakrishnan et al., 2022; Cao et al., 2024) are often described as mathematical forms, and digital circuits could also be built for further verification. Indeed, these discrete memristors have an important impact on the dynamics of neural circuits (Njitacke Tabekoueng et al., 2022; Bao BC et al., 2023; Shatnawi et al., 2023), and they have potential applications in signal processing and image encryption. When more neurons in map or oscillator form are clustered in a network (Majhi et al., 2022; Ji et al., 2023; Xie et al., 2023), the collective behaviors show complex characteristics and synchronization control becomes a challenge. Higher coupling between neurons leads to similar properties to those displayed by field coupling via hybrid synapse, and readers can find possible guidance in relevant reviews and studies (Parastesh et al., 2022; Guo et al., 2023a; Li et al., 2023; Ma, 2023). The scheme suggested here provides a theoretical approach for setting functional maps with clear definition of energy function.

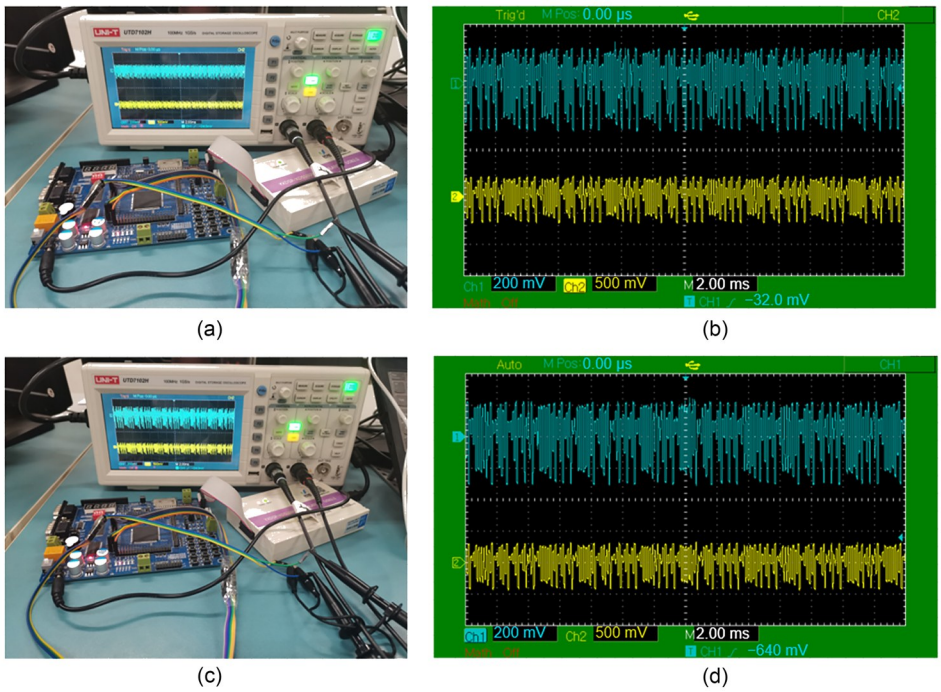

Fig. 14 Chaotic sequences of memristive maps implemented on a DSP platform of hardware device (a, c) and chaotic sequences (b, d) generated by the memristive maps presented in Eqs. (10) and (22), respectively

4 Conclusions

In this study, two simple memristive circuits were built to develop different memristive oscillators and discern the effect of the magnetic field and electric field. The energy functions for the memristive oscillators were obtained theoretically, and we discussed the relation to mode selection in detail. By applying linear transformation on the sampled variables for memristive oscillators, we were able to design two different memristive maps with clear definition of energy function. An adaptive growth law for parameters was proposed to explain the intrinsic self-adaptive property of neurons. The results indicate that both memristive maps have rich dynamic behaviors, and the dynamics can be adjusted in an adaptive way under energy flow. The maps have a smaller mean Hamilton energy value in a chaotic state, but maintain a higher mean Hamilton energy value in a periodic state. In addition, the mean Hamilton energy value of the memristive maps decreases as the period number increases. We implemented both memristive maps on a DSP platform. The results illustrate the effectiveness of discrete maps. In addition, these simple maps can be used for image-encryption fields and pseudo-random sequence generation.

Acknowledgments

This work is supported by the National Natural Science Foundation of China (No. 12072139).

Author contributions

Feifei YANG: methodology, software, numerical calculation, and writing-original draft. Lujie REN: numerical calculation and DSP implementation. Jun MA and Zhigang ZHU: methodology, supervision, and writing-final version.

Conflict of interest

Jun MA is an Editorial Board member of this journal, and is NOT involved in the editorial review or the decision to publish this article. Feifei YANG, Lujie REN, Jun MA, and Zhigang ZHU declare that they have no conflict of interest.

References

Bao BC, Li HZ, Wu HG, et al., 2020. Hyperchaos in a second order discrete memristor based map model. *Electronics Letters*, 56(15):769-770. https://doi.org/10.1049/el.2020.1172

Bao BC, Zhao QH, Yu XH, et al., 2023a. Complex dynamics and initial state effects in a two-dimensional sine-bounded memristive map. *Chaos, Solitons & Fractals*, 173:113748. https://doi.org/10.1016/j.chaos.2023.113748

Bao BC, Hu JT, Cai JM, et al., 2023b. Memristor-induced mode transitions and extreme multistability in a map-based neuron model. *Nonlinear Dynamics*, 111(4):3765-3779. https://doi.org/10.1007/s11071-022-07981-8

Bao H, Zhang YZ, Liu WB, et al., 2020. Memristor synapse-coupled memristive neuron network: synchronization transition and occurrence of chimera. *Nonlinear Dynamics*, 100(1):937-950. https://doi.org/10.1007/s11071-020-05529-2

Bao H, Chen ZG, Cai JM, et al., 2022. Memristive cyclic three-neuron-based neural network with chaos and global coexisting attractors. *Science China Technological Sciences*, 65(11):2582-2592. https://doi.org/10.1007/s11431-022-2144-x

Bao H, Li KX, Ma J, et al., 2023. Memristive effects on an improved discrete Rulkov neuron model. *Science China Technological Sciences*, 66(11):3153-3163. https://doi.org/10.1007/s11431-023-2432-1

Batas D, Fiedler H, 2011. A memristor SPICE implementation and a new approach for magnetic flux-controlled memristor modeling. *IEEE Transactions on Nanotechnology*, 10(2):250-255. https://doi.org/10.1109/TNANO.2009.2038051

Boybat I, le Gallo M, Nandakumar SR, et al., 2018. Neuromorphic computing with multi-memristive synapses. *Nature Communications*, 9(1):2514. https://doi.org/10.1038/s41467-018-04933-y

Cao HL, Wang Y, Banerjee S, et al., 2024. A discrete Chialvo–Rulkov neuron network coupled with a novel memristor model: design, dynamical analysis, DSP implementation and its application. *Chaos, Solitons & Fractals*, 179:114466. https://doi.org/10.1016/j.chaos.2024.114466

Chandía KJ, Bologna M, Tellini B, 2018. Multiple scale approach to dynamics of an LC circuit with a charge-controlled memristor. *IEEE Transactions on Circuits and Systems II: Express Briefs*, 65(1):120-124. https://doi.org/10.1109/TCSII.2017.2699423

Chen M, Qi JW, Wu HG, et al., 2020. Bifurcation analyses and hardware experiments for bursting dynamics in non-autonomous memristive Fitzhugh-Nagumo circuit. *Science China Technological Sciences*, 63(6):1035-1044. https://doi.org/10.1007/s11431-019-1458-5

Chua L, 1971. Memristor-the missing circuit element. *IEEE Transactions on Circuit Theory*, 18(5):507-519. https://doi.org/10.1109/TCT.1971.1083337

Covi E, Brivio S, Serb A, et al., 2016. Analog memristive synapse in spiking networks implementing unsupervised learning. *Frontiers in Neuroscience*, 10:482. https://doi.org/10.3389/fnins.2016.00482

Deng Y, Li YX, 2021. Bifurcation and bursting oscillations in 2D non-autonomous discrete memristor-based hyperchaotic map. *Chaos, Solitons & Fractals*, 150:111064. https://doi.org/10.1016/j.chaos.2021.111064

Deng Y, Li YX, 2022. A 2D hyperchaotic discrete memristive map and application in reservoir computing. *IEEE Transactions on Circuits and Systems II: Express Briefs*, 69(3):1817-1821.

https://doi.org/10.1109/TCSII.2021.3118646

Fan ZY, Zhang CK, Wang YM, et al., 2023. Construction, dynamic analysis and DSP implementation of a novel 3D discrete memristive hyperchaotic map. *Chaos, Solitons & Fractals*, 177:114303. https://doi.org/10.1016/j.chaos.2023.114303

Gokyildirim A, Yesil A, Babacan Y, 2022. Implementation of a memristor-based 4D chaotic oscillator and its nonlinear control. *Analog Integrated Circuits and Signal Processing*, 110(1):91-104. https://doi.org/10.1007/s10470-021-01956-2

Guo YT, Yao Z, Xu Y, et al., 2022. Control the stability in chaotic circuit coupled by memristor in different branch circuits. *AEU-International Journal of Electronics and Communications*, 145:154074. https://doi.org/10.1016/j.aeue.2021.154074

Guo YT, Xie Y, Wang CN, et al., 2023a. Energy and synchronization between two neurons with nonlinear coupling. *Cognitive Neurodynamics*, in press. https://doi.org/10.1007/s11571-023-10044-2

Guo YT, Xie Y, Ma J, 2023b. How to define energy function for memristive oscillator and map? *Nonlinear Dynamics*, 111(23):21903-21915. https://doi.org/10.1007/s11071-023-09039-9

Hoang DV, Dong CST, van Huynh V, et al., 2023. Building discrete maps with memristor and multiple nonlinear terms. *Integration*, 90:126-130. https://doi.org/10.1016/j.vlsi.2023.01.013

Hou B, Hu XK, Guo YT, et al., 2023. Energy flow and stochastic resonance in a memristive neuron. *Physica Scripta*, 98(10):105236. https://doi.org/10.1088/1402-4896/acf89a

Ibarz B, Casado JM, Sanjuán MAF, 2011. Map-based models in neuronal dynamics. *Physics Reports*, 501(1-2):1-74. https://doi.org/10.1016/j.physrep.2010.12.003

Isah A, Nguetcho AST, Binczak S, et al., 2020. Dynamics of a charge controlled memristor in master–slave coupling. *Electronics Letters*, 56(4):211-213. https://doi.org/10.1049/el.2019.3322

Ji P, Ye JC, Mu Y, et al., 2023. Signal propagation in complex networks. *Physics Reports*, 1017:1-96. https://doi.org/10.1016/j.physrep.2023.03.005

Juzekaeva E, Nasretdinov A, Battistoni S, et al., 2019. Coupling cortical neurons through electronic memristive synapse. *Advanced Materials Technologies*, 4(1):1800350. https://doi.org/10.1002/admt.201800350

Lai Q, Yang L, 2023. A new 3-D memristive hyperchaotic map with multi-parameter-relied dynamics. *IEEE Transactions on Circuits and Systems II: Express Briefs*, 70(4):1625-1629. https://doi.org/10.1109/TCSII.2022.3225919

Li CL, Yang YY, Du JR, et al., 2021. A simple chaotic circuit with magnetic flux-controlled memristor. *The European Physical Journal Special Topics*, 230(7):1723-1736. https://doi.org/10.1140/epjs/s11734-021-00181-2

Li XQ, Ghosh D, Lei YM, 2023. Chimera states in coupled pendulum with higher-order interaction. *Chaos, Solitons & Fractals*, 170:113325. https://doi.org/10.1016/j.chaos.2023.113325

Lin HR, Wang CH, Xu C, et al., 2023. A memristive synapse control method to generate diversified multistructure chaotic attractors. *IEEE Transactions on Computer-Aided Design of Integrated Circuits and Systems*, 42(3):942-955. https://doi.org/10.1109/TCAD.2022.3186516

Liu Y, Iu HHC, Qian YH, 2021. Implementation of Hodgkin-Huxley neuron model with the novel memristive oscillator. *IEEE Transactions on Circuits and Systems II: Express Briefs*, 68(8):2982-2986. https://doi.org/10.1109/TCSII.2021.3066471

Liu ZL, Yu Y, Wang QY, 2022a. Functional modular organization unfolded by chimera-like dynamics in a large-scale brain network model. *Science China Technological Sciences*, 65(7):1435-1444. https://doi.org/10.1007/s11431-022-2025-0

Liu ZL, Han F, Wang QY, 2022b. A review of computational models for gamma oscillation dynamics: from spiking neurons to neural masses. *Nonlinear Dynamics*, 108(3):1849-1866. https://doi.org/10.1007/s11071-022-07298-6

Luo LQ, Flanagan JG, 2007. Development of continuous and discrete neural maps. *Neuron*, 56(2):284-300. https://doi.org/10.1016/j.neuron.2007.10.014

Ma J, 2023. Biophysical neurons, energy, and synapse controllability: a review. *Journal of Zhejiang University-SCIENCE A (Applied Physics & Engineering)*, 24(2):109-129. https://doi.org/10.1631/jzus.A2200469

Ma J, 2024. Energy function for some maps and nonlinear oscillators. *Applied Mathematics and Computation*, 463:128379. https://doi.org/10.1016/j.amc.2023.128379

Ma ML, Yang Y, Qiu ZC, et al., 2022. A locally active discrete memristor model and its application in a hyperchaotic map. *Nonlinear Dynamics*, 107(3):2935-2949. https://doi.org/10.1007/s11071-021-07132-5

Ma YJ, Mou J, Lu JS, et al., 2023. A discrete memristor coupled two-dimensional generalized square hyperchaotic maps. *Fractals*, 31(6):2340136. https://doi.org/10.1142/S0218348X23401369

Majhi S, Perc M, Ghosh D, 2022. Dynamics on higher-order networks: a review. *Journal of the Royal Society Interface*, 19(188):20220043. https://doi.org/10.1098/rsif.2022.0043

Mehrabbeik M, Jafari S, Perc M, 2023. Synchronization in simplicial complexes of memristive Rulkov neurons. *Frontiers in Computational Neuroscience*, 17:1248976. https://doi.org/10.3389/fncom.2023.1248976

Njimah OM, Ramadoss J, Telem ANK, et al., 2023. Coexisting oscillations and four-scroll chaotic attractors in a pair of coupled memristor-based Duffing oscillators: theoretical analysis and circuit simulation. *Chaos, Solitons & Fractals*, 166:112983. https://doi.org/10.1016/j.chaos.2022.112983

Njitacke Tabekoueng Z, Shankar Muni S, Fonzin Fozin T, et al., 2022. Coexistence of infinitely many patterns and their control in heterogeneous coupled neurons through a multistable memristive synapse. *Chaos: an Interdisciplinary*

Journal of Nonlinear Science, 32(5):053114. https://doi.org/10.1063/5.0086182

Parastesh F, Mehrabbeik M, Rajagopal K, et al., 2022. Synchronization in Hindmarsh–Rose neurons subject to higher-order interactions. *Chaos: an Interdisciplinary Journal of Nonlinear Science*, 32(1):013125. https://doi.org/10.1063/5.0079834

Pedretti G, Milo V, Ambrogio S, et al., 2017. Memristive neural network for on-line learning and tracking with brain-inspired spike timing dependent plasticity. *Scientific Reports*, 7(1):5288. https://doi.org/10.1038/s41598-017-05480-0

Pham VT, Jafari S, Vaidyanathan S, et al., 2016. A novel memristive neural network with hidden attractors and its circuitry implementation. *Science China Technological Sciences*, 59(3):358-363. https://doi.org/10.1007/s11431-015-5981-2

Pham VT, Velichko A, van Huynh V, et al., 2024. Analysis of memristive maps with asymmetry. *Integration*, 94:102110. https://doi.org/10.1016/j.vlsi.2023.102110

Ramadoss J, Ouannas A, Tamba VK, et al., 2022. Constructing non-fixed-point maps with memristors. *The European Physical Journal Plus*, 137(2):211. https://doi.org/10.1140/epjp/s13360-022-02433-z

Ramakrishnan B, Mehrabbeik M, Parastesh F, et al., 2022. A new memristive neuron map model and its network's dynamics under electrochemical coupling. *Electronics*, 11(1):153. https://doi.org/10.3390/electronics11010153

Ren LJ, Mou J, Banerjee S, et al., 2023. A hyperchaotic map with a new discrete memristor model: design, dynamical analysis, implementation and application. *Chaos, Solitons & Fractals*, 167:113024. https://doi.org/10.1016/j.chaos.2022.113024

Shatnawi MT, Khennaoui AA, Ouannas A, et al., 2023. A multistable discrete memristor and its application to discrete-time Fitzhugh–Nagumo model. *Electronics*, 12(13):2929. https://doi.org/10.3390/electronics12132929

Smagulova K, James AP, 2019. A survey on LSTM memristive neural network architectures and applications. *The European Physical Journal Special Topics*, 228(10):2313-2324. https://doi.org/10.1140/epjst/e2019-900046-x

Sun JW, Yang JL, Liu P, et al., 2023. Design of general flux-controlled and charge-controlled memristor emulators based on hyperbolic functions. *IEEE Transactions on Computer-Aided Design of Integrated Circuits and Systems*, 42(3):956-967. https://doi.org/10.1109/TCAD.2022.3186928

Vignesh D, Ma J, Banerjee S, 2024. Multi-scroll and coexisting attractors in a Hopfield neural network under electromagnetic induction and external stimuli. *Neurocomputing*, 564:126961. https://doi.org/10.1016/j.neucom.2023.126961

Wang ZR, Joshi S, Savel'ev S, et al., 2018. Fully memristive neural networks for pattern classification with unsupervised learning. *Nature Electronics*, 1(2):137-145. https://doi.org/10.1038/s41928-018-0023-2

Wu FQ, Yao Z, 2023. Dynamics of neuron-like excitable Josephson junctions coupled by a metal oxide memristive synapse. *Nonlinear Dynamics*, 111(14):13481-13497. https://doi.org/10.1007/s11071-023-08524-5

Wu FQ, Guo YT, Ma J, 2022. Reproduce the biophysical function of chemical synapse by using a memristive synapse. *Nonlinear Dynamics*, 109(3):2063-2084. https://doi.org/10.1007/s11071-022-07533-0

Wu FQ, Guo YT, Ma J, 2023. Energy flow accounts for the adaptive property of functional synapses. *Science China Technological Sciences*, 66(11):3139-3152. https://doi.org/10.1007/s11431-023-2441-5

Xie Y, Yao Z, Ma J, 2023. Formation of local heterogeneity under energy collection in neural networks. *Science China Technological Sciences*, 66(2):439-455. https://doi.org/10.1007/s11431-022-2188-2

Xu Q, Lin Y, Bao BC, et al., 2016. Multiple attractors in a non-ideal active voltage-controlled memristor based Chua's circuit. *Chaos, Solitons & Fractals*, 83:186-200. https://doi.org/10.1016/j.chaos.2015.12.007

Xu Q, Huang LP, Wang N, et al., 2023. Initial-offset-boosted coexisting hyperchaos in a 2D memristive Chialvo neuron map and its application in image encryption. *Nonlinear Dynamics*, 111(21):20447-20463. https://doi.org/10.1007/s11071-023-08905-w

Yang FF, Wang Y, Ma J, 2023a. Creation of heterogeneity or defects in a memristive neural network under energy flow. *Communications in Nonlinear Science and Numerical Simulation*, 119:107127. https://doi.org/10.1016/j.cnsns.2023.107127

Yang FF, Ren GD, Tang J, 2023b. Dynamics in a memristive neuron under an electromagnetic field. *Nonlinear Dynamics*, 111(23):21917-21939. https://doi.org/10.1007/s11071-023-08969-8

Yang FF, Xu Y, Ma J, 2023c. A memristive neuron and its adaptability to external electric field. *Chaos: an Interdisciplinary Journal of Nonlinear Science*, 33(2):023110. https://doi.org/10.1063/5.0136195

Ye XL, Wang XY, Gao S, et al., 2020. A new chaotic circuit with multiple memristors and its application in image encryption. *Nonlinear Dynamics*, 99(2):1489-1506. https://doi.org/10.1007/s11071-019-05370-2

Yu Y, Fan YB, Han F, et al., 2023. Transcranial direct current stimulation inhibits epileptic activity propagation in a large-scale brain network model. *Science China Technological Sciences*, 66(12):3628-3638. https://doi.org/10.1007/s11431-022-2341-x

Zandi-Mehran N, Panahi S, Hosseini Z, et al., 2020. One dimensional map-based neuron model: a phase space interpretation. *Chaos, Solitons & Fractals*, 132:109558. https://doi.org/10.1016/j.chaos.2019.109558

Zhao Y, Ding JF, He SB, et al., 2023. Fully fixed-point integrated digital circuit design of discrete memristive systems. *AEU-International Journal of Electronics and Communications*, 161:154522. https://doi.org/10.1016/j.aeue.2022.154522

Zhong HY, Li GD, Xu XL, 2022. A generic voltage-controlled discrete memristor model and its application in chaotic map. *Chaos, Solitons & Fractals*, 161:112389. https://doi.org/10.1016/j.chaos.2022.112389